AD-A034 795 AEL SERVICE CORP FARMINGDALE N J F/G 20/3
ELECTROMAGNETIC RADIATION SYSTEM (EMRS) FOR SUSCEPTIBILITY TEST--ETC(U)
DEC 76 E S ISKRA DAAB07-76-C-0332
UNCLASSIFIED AELSC-TR-23-2 ECOM-76-0332-2 NL

1 OF 1
AD A034795

END
DATE FILMED
2-77

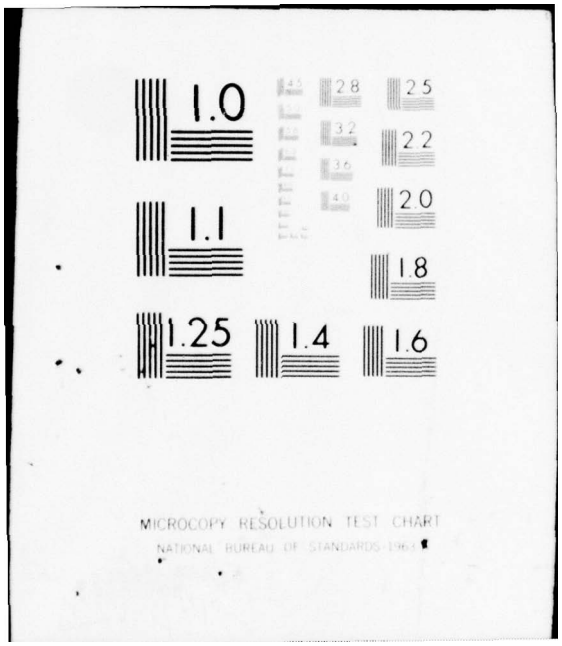
1.0
1.1
1.25
1.4
1.6
2.8
2.5
3.2
2.2
3.6
2.0
4.0
1.8
MICROCOPY RESOLUTION TEST CHART
NATIONAL BUREAU OF STANDARDS-1963

(12)

FG.

Research and Development Technical Report

ECOM- 76-0332-2

ELECTROMAGNETIC RADIATION SYSTEM (EMRS)

FOR SUSCEPTIBILITY TESTING

Edwin S. Iskra
American Electronic Laboratories, Inc.
P. O. Box 691
Farmingdale, NJ 07727

December 1976

Quarterly Report for Period 2 February 1976 - 30 April 1976

DISTRIBUTION STATEMENT

APPROVED FOR PUBLIC RELEASE;

DISTRIBUTION UNLIMITED

PREPARED FOR:
COMMUNICATION/ADP LABORATORY
DRSEL-NL-RY-5

ECOM

US ARMY ELECTRONICS COMMAND FORT MONMOUTH, NEW JERSEY 07703

NOTICES

Disclaimers

The findings in this report are not to be construed as an official Department of the Army position, unless so designated by other authorized documents.

The citation of trade names and names of manufacturers in this report is not to be construed as official Government endorsement or approval of commercial products or services referenced herein.

Disposition

Destroy this report when it is no longer needed. Do not return it to the originator.

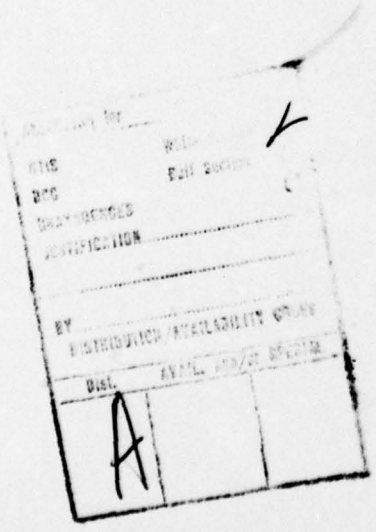

Research and Development Technical Report

ECOM- 76-0332-2

ELECTROMAGNETIC RADIATION SYSTEM (EMRS)

FOR SUSCEPTIBILITY TESTING

Edwin S. Iskra
American Electronic Laboratories, Inc.
P. O. Box 691
Farmingdale, NJ 07727

December 1976

Quarterly Report for Period 2 February 1976 - 30 April 1976

DISTRIBUTION STATEMENT

APPROVED FOR PUBLIC RELEASE;

DISTRIBUTION UNLIMITED

PREPARED FOR:
COMMUNICATION/ADP LABORATORY
DRSEL-NL-RY-5

ECOM

US ARMY ELECTRONICS COMMAND FORT MONMOUTH, NEW JERSEY 07703

See 1423

UNCLASSIFIED

SECURITY CLASSIFICATION OF THIS PAGE (When Data Entered)

REPORT DOCUMENTATION PAGE	READ INSTRUCTIONS BEFORE COMPLETING FORM
1. REPORT NUMBER (18) (19) ECOM-76-0332-2 ✓	2. GOVT ACCESSION NO.
3. RECIPIENT'S CATALOG NUMBER	
4. TITLE (and Subtitle) (6) ELECTROMAGNETIC RADIATION SYSTEM (EMRS) FOR SUSCEPTIBILITY TESTING. ✓	5. TYPE OF REPORT & PERIOD COVERED (9) Quarterly Report. no. 2, 2 Feb 30 Apr 76,
6. PERFORMING ORG. REPORT NUMBER (14) AELSC-TR-23-2 ✓	
7. AUTHOR(s) (10) Edwin S. Iskra, American Electronic Laboratories, Inc.	8. CONTRACT OR GRANT NUMBER(s) (15) DAABØ7-76-C-Ø332 ✓
9. PERFORMING ORGANIZATION NAME AND ADDRESS American Electronic Laboratories, Inc. ? P. O. Box 691 AEL Service Corp - Farmingdale, NJ 07727 per item fourteen	10. PROGRAM ELEMENT, PROJECT, TASK AREA & WORK UNIT NUMBERS 6.27.01.A 1L7 62701 AH92 C1 071 C8
11. CONTROLLING OFFICE NAME AND ADDRESS Communications/ADP Laboratory DRSEL-NL-RY-5 U.S. Army Electronics Command Fort Monmouth, New Jersey 07703	12. REPORT DATE (11) December 1976
	13. NUMBER OF PAGES 44 (12) 50 P.
14. MONITORING AGENCY NAME & ADDRESS (if different from Controlling Office) (16) 1L7627ØIAH92 (12) C1	15. SECURITY CLASS. (of this report) UNCLASSIFIED
	15a. DECLASSIFICATION/DOWNGRADING SCHEDULE

16. DISTRIBUTION STATEMENT (of this Report)

Approved for public release; distribution unlimited.

17. DISTRIBUTION STATEMENT (of the abstract entered in Block 20, if different from Report)

18. SUPPLEMENTARY NOTES

19. KEY WORDS (Continue on reverse side if necessary and identify by block number)

Electromagnetic Compatibility, electromagnetic-energy.
Electromagnetic Radiation System
(EMRS)

20. ABSTRACT (Continue on reverse side if necessary and identify by block number)

The function of the Electromagnetic Radiation System (EMRS) is to generate electromagnetic energy so as to produce a constant field strength that can be automatically scanned as a function of frequency. The design objective is to cover the frequency range of 30 hertz to 40 gigahertz with field strength intensities up to 200 volts per meter. A stripline approach is described and proposed for use as the field generating device for the

409 710

DD FORM 1 JAN 73 1473 EDITION OF 1 NOV 65 IS OBSOLETE

UNCLASSIFIED

SECURITY CLASSIFICATION OF THIS PAGE (When Data Entered)

lower frequencies. The use of defocused parabolas are proposed for use at the higher frequencies.

TABLE OF CONTENTS

INTRODUCTION

System Evaluation

A conclusion reached in the first quarterly report was to use a parallel-plate structure and an elliptical reflector as the field generating devices at the low and high frequencies, respectively. Although the advantages of the two systems as described in the first quarterly report are substantial compared to other alternatives, both approaches would result in bulky structures when large test objects are to be irradiated.

During this second quarter reporting period, new techniques have evolved and are analyzed in the Field Generation section of this report.

Total System Concept

It is conceivable that the EMRS might be, at a future time, integrated with an automatically scanned receiving system to provide a total automated EMI emission/susceptibility test facility. Therefore, it is desirable to consider the total system concept as it may impact on the subsystem design, in this case, the EMRS or signal generation portion of the total EMI instrumentation system.

In a fully automated system, with integrated amplitude-frequency scanning, it is necessary to synchronize the transmitting and receiving frequencies. The advantages of such a system are:

- speed of operation (fast scanning and plotting)
- minimize human intervention and error
- accuracy and reliability
- self-calibration
- diversified user capability
- updating capability
- automatic analysis of results

Ideally, the system would minimize data reduction requirements and determine cause and effect by incorporating decision making capability based on intelligent interpretation of pre-set limits and documented results corresponding to controlled changes in the operating characteristics of the test objects. Such a system would then require statistical analysis to convert data to probability displays and an automatic signal convergence in various test modes.

The total system synchronization should therefore beconsidered in the present EMRS design as applicable to future applications in fully automated systems. Figure 1 shows two practical schemes for frequency tracking and, equipment-wise, the two are equivalent. Figure 1(a) is preferred, however, because the generating portion of this system can be used with all receivers, synchronized or not, and also because the selection of the intermediate frequency and the mixing process are receiver design criteria. The EMRS generating equipment will, therefore, incorporate the signal generating circuitry, and subsequent receiver designs should address themselves to the frequency lock mixing function.

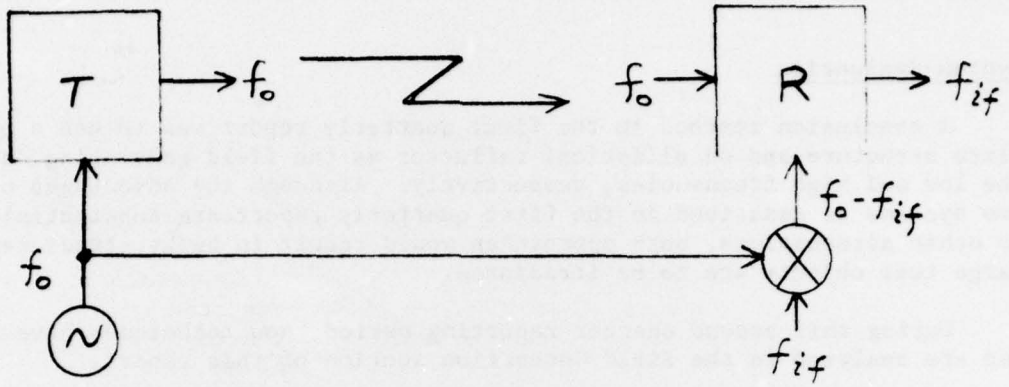

(a) RECEIVER SLAVE TO TRANSMITTER

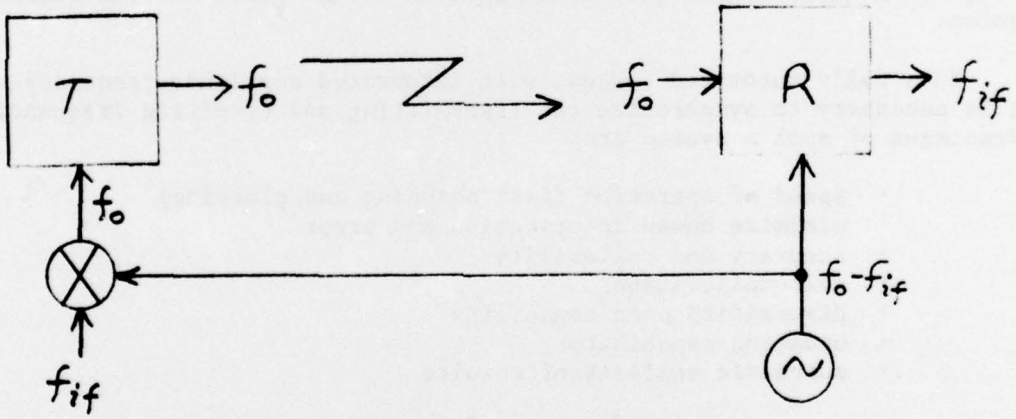

(b) TRANSMITTER SLAVE TO RECEIVER

⊗ = MIXER

~ = GENERATOR

T = TRANSMITTER
R = RECEIVER
f_o = OPERATING FREQUENCY
f_{if} = RECEIVER INTERMEDIATE FREQUENCY

FIGURE 1

FREQUENCY TRACKING SYSTEMS

FIELD GENERATION

Approach

During this reporting period, a stripline approach evolved as a "limiting" type application of the parallel plate approach. Also, further consideration of the elliptic reflector approach was discontinued because of its complexity. The presently envisioned approaches to the field producing devices are the stripline and defocused parabolas.

One problem with the parallel plate line is the size; large, widely separated plates are required to measure large test objects. The wide separation also limits the high frequency usefulness of the parallel plate line. When a large test object is placed between the plates, the separation between the test object and the plates becomes small. If the test object is located such that it is on the ground plate, the test object and the field generating system are at the same ground potential. The net effect is a "hot" conductor some small distance above a ground plane. This is the configuration for a microstrip transmission line.

As originally conceived, the elliptic reflector was to be used down to 400 MHz as a minimum because of the frequency limitation of the parallel plate line. With the advent of the proposed stripline tape, a system to cover the 400 MHz to 2 GHz range is no longer necessary. This is significant since the size of the reflector at the low frequencies becomes a major obstacle in the implementation of the elliptic reflector design.

Above 2 GHz, reflector sizes become more realizable with the problem of the standard parabola being that it focuses energy at infinity rather than at 3 meters or closer. The advantage of the elliptic reflector is that any energy radiated from the first focus is reflected through the second focus.

An analysis of the path length dispersion of energy which is refocused by an ellipsoid segment is given in the Appendix. This analysis concluded that although focusing of the energy occurs at the second focal point, it cannot produce higher power densities than those existing in the feed beam of the source aperture located at the first focal point. Consequently, a defocused parabola exhibits characteristics similar to those of an ellipsoid segment without resorting to complex geometrics and special reflector design and fabrication. An article by Cheng* offers a solution from an ellipsoidal reflector. He goes about this by showing that "... an ellipsoidal reflector of focal lengths f_1 and f_2 approximates a paraboloidal reflector of focal length f...".

*D.K. Cheng; Defocus Characteristics of Microwave Reflectors; ASTIA Document, AD 98167, 1955, Syracuse University.

Microstrip

As a result of the continuing work effort on the EMRS program, a new technique has evolved using microstrip transmission line. The microstrip will be formed by printing a conductor on a dielectric material and then positioning this on the test object using the conductive surface of the test object as the ground plane for the microstrip transmission line. E fields will then be generated between the conductor and the test object. By simulating such a transmission line structure around the test object, the entire test object will be subjected to these fields.

This approach has a number of advantages. There is no chamber required since the fields exist only between the conductor and the test object. The power required to generate a 200 V/m field is much less than that for a Crawford Cell or parallel plate waveguide since the separation between the conductor and ground is considerably less. Also, with proper implementation, simultaneous multi-face excitation of the test object can be affected.

Of immediate interest is the equivalency of the microstrip approach with that of subjecting the test object to a radiated field. Figure 2 shows the equivalent normally incident (freespace) radiative field for surface currents induced in a metal wall by a parallel running transmission line strip. This forms the basis for the following calculations. The main result to be obtained, equation (10) does not depend upon the dielectric constant of non-magnetic material between the strip and the wall, nor upon whether an outside shield strip is used with the line; only the drive power is affected by these factors.

Because h is assumed to be much less than ℓ, the surface current density induced on the metal wall will be about equal to that on the wall-facing side of the "hot" strip:

$$K = I/\ell \qquad \text{(Amperes/meter)} \qquad (1)^*$$

The surface-directed magnetic field, H, is closely given by:

$$H = K \qquad \text{(Amperes/meter)} \qquad (2)^+$$

By simple substitution:

$$H = I/\ell \qquad \text{(Amperes/meter)} \qquad (3)$$

The incident free-space wave magnetic field H_i that would be needed, to produce the same boundary magnetic field H (and, hence, the same surface-current density) upon full reflection of the wave, is:

$$H_i = H/2 \qquad (4)$$

* ITT; Reference Data for Radio Engineers, Fifth Edition; page 3-14.

\+ E.C. Jordan; Electromagnetic Waves and Radiating Systems; Equation (3-8)

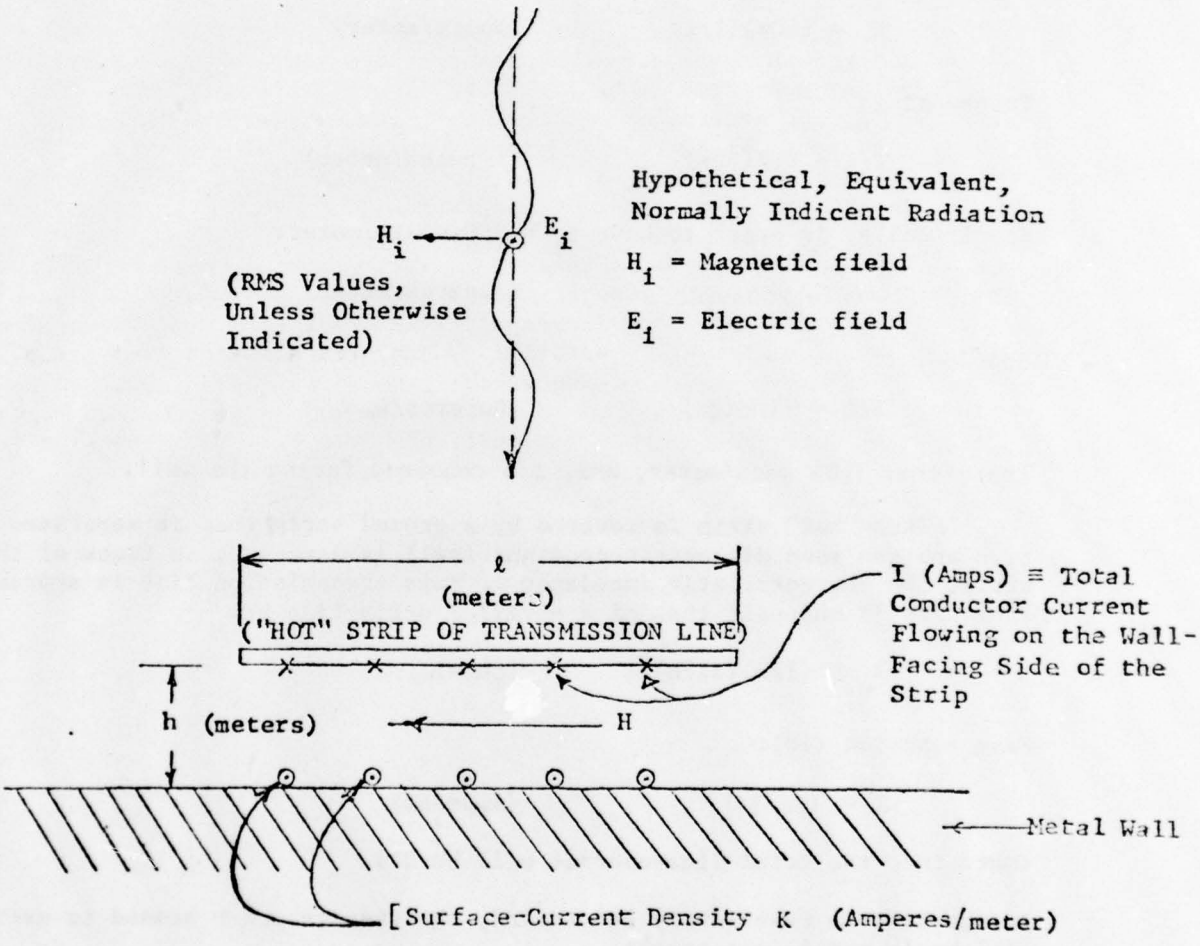

NOTE: $h \ll \ell$

FREE SPACE INCIDENT

AND MICROSTRIP FIELDS

FIGURE 2

Substituting equation (3) in equation (4):

$$H_i = I/(2\ell) \qquad \text{(Amperes/meter)} \qquad (5)$$

The fields of travelling plane electromagnetic wave are related by:

$$E_i = (120\pi)H_i \qquad \text{(Volts/meter)} \qquad (6)^*$$

Substituting equation (5) in equation (6):

$$E_i = (60\pi)(I/\ell) \qquad \text{(Volts/meter)} \qquad (7)$$

Transposing:

$$I/\ell = E_i/(60\pi) \qquad \text{(Amperes/meter)} \qquad (8)$$

Specifically, in order to have E_i = 200 volts/meter:

$$I/\ell = 200/(60\pi) \qquad \text{(Amperes/meter)} \qquad (9)$$

Solving:

$$I/\ell = 10/(3\pi) \qquad \text{(Amperes/meter)} \qquad (10)$$

Therefore, 1.06 amps/meter, RMS, are required facing the wall.

If the "hot" strip is covered by a ground strip that is separated from it by h and the same dielectric-constant (ϵ=1) is used on both faces of the hot strip, the characteristic impedance of this transmission line is approximately (for $h/\ell << 1$) one-half that of a parallel strip line or:

$$Z_o \simeq (1/2)(377h)/\ell \qquad \text{(Ohms)} \qquad (11)^+$$

From equation (10):

$$I = 10\ell/3\pi) \qquad \text{(Amperes)} \qquad (12)$$

(Note that the total line-current will be 2I).

If the line is resistively terminated, the average power needed to excite it will be (h and ℓ in meters):

$$W = (2I)^2 Z_o = 848.8h\ell \qquad \text{(Watts)} \qquad (13)$$

It is interesting to compare the power density in the line with the power density of the equivalent incoming wave: The cross-sectional area of the line is $(2h\ell)$, hence the line's power density P_ℓ, from (13) is:

$$P_\ell = W/(2h\ell) = 424.4 \qquad \text{(Watts/square meter)} \qquad (14)$$

* E.C. Jordan, Electromagnetic Waves and Radiating Systems; Equation (5-22).

\+ ITT: Reference Data for Radio Engineers, Fifth Edition; page 22-22.

The average Poynting-flux P_o of an incoming-wave is:

$$P_o = |E_i H_i| \qquad (15)^*$$

With E_i = 200 volts/meter and substituting equation (6):

$$P_o = 106.1 \quad \text{(Watts/square meter)} \qquad (16)$$

Therefore:

$$P_\ell / P_o = 424.4/106.1 = 4 \qquad (17)$$

The power density in the transmission line is 4 times that of the free-space normally incident wave (this is as should be expected, because, both are TEM, and the line's H must be twice the incident wave's H_i).

An experiment was performed to verify the preceding analysis and to determine the feasibility of the stripline tape concept. The experiment consisted of constructing a 1 x 1 x 1 foot conductive cube with a slot aperture cut into it. The slot dimensions were .85 x 1.9 inches. A waveguide adapter with the same dimension as the slot was mounted on the inside of the box such that its aperture was aligned with the aperture in the box. The stripline tape was formed by removing the outer conductor of UT-141 cable. This stripped coax was then wrapped around the box in two configurations as shown in Figure 3.

The test set-up is shown in Figure 4. The signal generator provided an RF signal at a frequency of 4 GHz with one thousand cycle modulation. The crystal detector of junction B was connected directly to the signal generator output of junction A and the SWR meter was set to a reference level of 0 dB. Then the RF signal was fed into the "stripline" and the detector was connected to the adapter output as shown in Figure 4. The magnitude of coupling was then determined by noting the relative signal level indicated by the SWR meter. This procedure was used for both wrap configurations shown in Figure 3. For the horizontal configuration (Figure 3), the lines were approximately .25 inches out from the edge of the slot, and the energy coupled into the slot was 30 dB lower than the reference signal level. For the vertical configuration (Figure 3), the adjacent lines were spaced 1.25 inches and the measured coupling was 15 dB below the reference.

To determine an equivalence to radiative techniques, a 2-5 GHz horn (AEL Model H-5101) was used to transmit a signal towards the test box with the slot cut in it. A reference level of 0 dB was established as in the first part of the experiment and then the RF signal was fed into the horn in the detector connected to the waveguide adapter as before. When the antenna was nine inches from the slot, with matched polarization to the slot, the energy received by the slot was -15 dB. For cross polarization, the received energy level was -30 dB with respect to the reference.

The results indicated that it is feasible to couple energy into a discontinuity in a conductive surface, in this case a slot, using the stripline tape approach. The equivalency between the stripline tape and radiative techniques was also demonstrated.

*E.C. Jordan; Electromagnetic Waves and Radiating Systems; Equation (6-8).

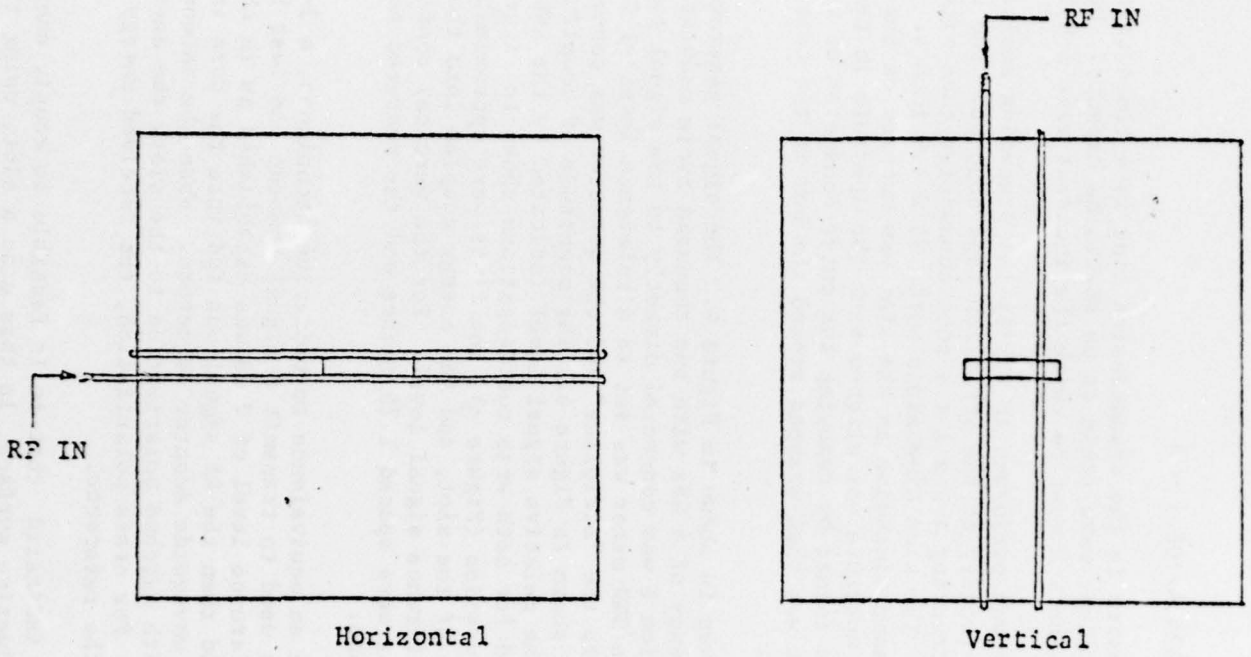

Figure 3. Wrap Configurations

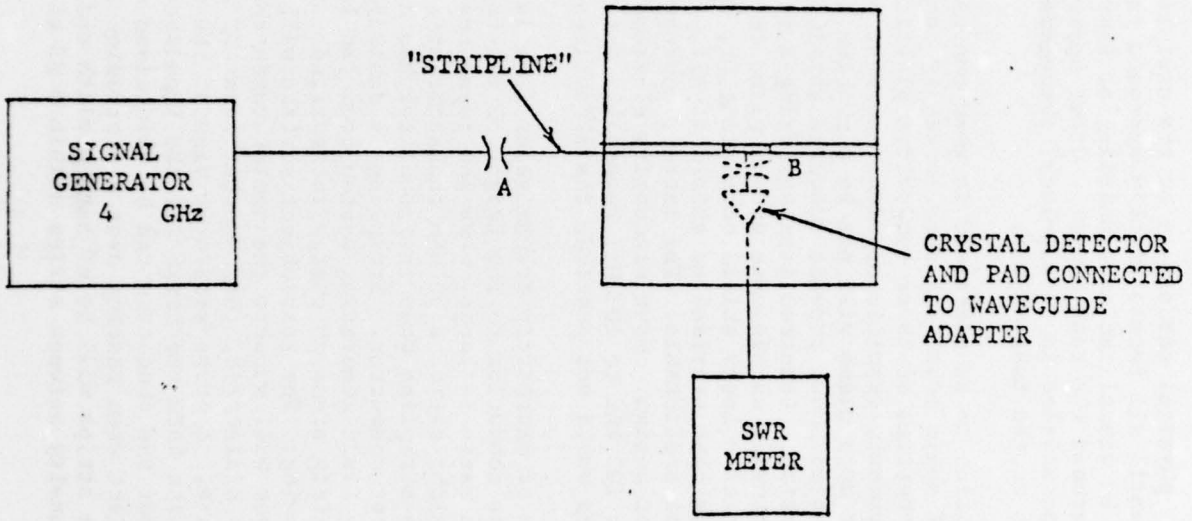

Figure 4. Test Set-Up

Stripline

The stripline approach represents a unique and innovative solution to the problem of field generation. The major advantages of this technique over conventional techniques is the small size and the relatively low power required to generate a 200 V/m field.

The practical physical embodiment of the stripline for this application must be reserved until all facets of this approach can be considered. Feasibly, the stripline can be visualized as consisting of flexible strips wrapped in successive turns around the test object. Other approaches are to utilize rigid strips which are paralleled in a "zip-lock" arrangement or to use rigid sheets to cover each face of the test object.

One consideration to be addressed is when the case of the test object is not constructed of solid metal but some partially conductive plastic. Since the electrical properties of these conductive plastics may vary and the effects are frequency dependent, specific applications must be considered. A general conclusion is that such cases will not be a problem if it is reasoned that the case of the test object must provide adequate shielding in order to accomplish its operating function. Constructions utilizing a strip mesh or random metal chips in plastic provide an adequate ground plane for stripline. If the construction consists of a lossy shield consisting of, for example, carbon in phenolic, or if the case provided no shield at all, the fields generated in these cases are not predictable. The latter, however, is highly unlikely in practical equipment design. Most conductive elastomers have good shielding effectiveness from 100 kHz to 10 GHz; reasonable deterioration outside of this band of frequencies would not preclude the effectiveness of the stripline.

The impedance of microstrip transmission line is a function of the ratio of the width of the conductor to the height of the conductor above the test object. When this ratio is large, very low impedances result. By choosing the proper width to height ratio, a 50 ohm characteristic impedance can be produced. Microstrip becomes stripline when the conductor has a ground plane both above and below the center conductor. Stripline is desirable because the outer ground plane isolates the field generating system from the local environment and provides personnel safety since no energy is radiated. The stripline will be composed of the following: The test object surface will provide the one ground plane, flexible foam will support the center conductor which will possibly be printed on another dielectric, then another layer of flexible foam will support the top ground plane. A cross-sectional view of the stripline can be found in Figures 5 and 6 which form the basis for the impedance calculations. A flexible foam is used so that the conductor can be maintained at a nearly constant height above the test object when passing over a protrusion to keep impedance variation to a minimum. The strips will be of such a width and have such a spacing as to provide field intensity between strips within 3 dB of 200 V/m as shown in Figure 6.

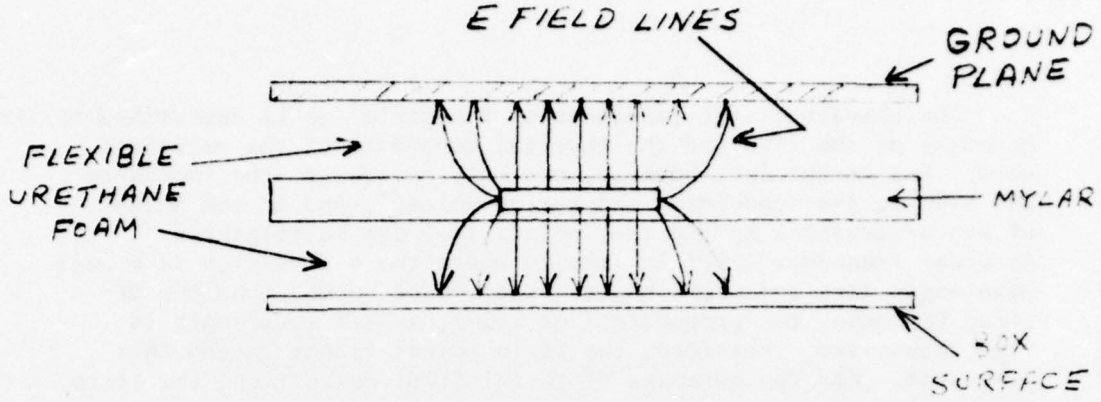

FIGURE 5

STRIPLINE CONFIGURATION

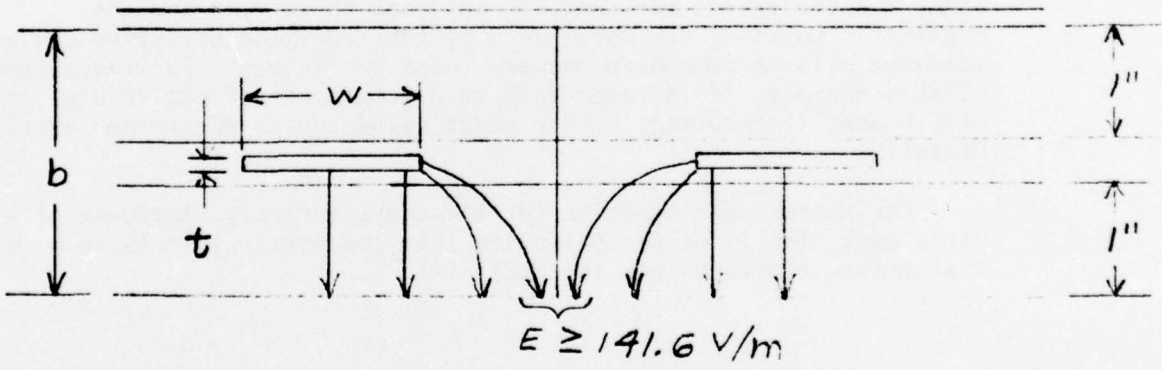

FIGURE 6

STRIPLINE FIELDS

The characteristic impedance of the stripline is determined by the geometry of the line and the physical constants of the materials used. The height (b), however, not only relates to the impedance but also to the bandwidth, excitation voltage, and to the height of any protrusions on the test object that can be tolerated. An upper frequency limit is imposed where the b dimension is a half wavelength long and where higher order modes, other than the desired TEM mode, can propogate. At 2 GHz, a half wavelength is 2.95 inches and, therefore, the strip height cannot exceed this dimension. For the purposes of this initial definition, the strip height above the test object ground plane is specified as 1 inch; this is considered to be a height that most protrusions on a typical test object will not exceed.

As an example, the flexible urethane foam, shown in Figure 5, is specified as the flexible, low loss, closed cell foam, Eccofoam PP, manufactured by Emerson & Cummings. This material has a dielectric constant of 1.15 and comes in 1 inch thicknesses. The configuration of the dielectric region shown in Figure 5 is two 1 inch thick layers of Eccofoam PP separated by a 0.1 inch thick layer of mylar. Since the dielectric constant for Eccofoam PP is 1.15 and the dielectric constant for mylar is 3.0, the resulting effective dielectric constant will be somewhere between these two values. For the purposes of this example, it is reasonable to assume a net effective dielectric of 1.6 and, if required, a more exact value can be determined experimentally.

The approximate equation for the characteristic impedance of wide strip stripline (wide strip implies that the strip width is so wide that fringe fields do not interact) is:

$$Z_o \sqrt{\varepsilon} = \frac{94.15}{\left(\frac{w/b}{1-t/b} + \frac{C}{.0885\varepsilon}\right)}$$

and

$$C = \frac{.0885\varepsilon}{\pi}\left[\frac{2}{1-t/b}\ln\left(\frac{1}{1-t/b}+1\right) - \left(\frac{1}{1-t/b}-1\right)\ln\left(\frac{1}{(1-t/b)^2}-1\right)\right] \text{ pf/cm} \qquad (18)^*$$

*H. Howe; Stripline Circuit Design; ARTECH House, Dedham, Mass., 1974; page 35.

where: t = Thickness of center conductor

w = Width of center conductor

b = Separation between ground planes

If $\varepsilon = 1.6$, b = 2.1 inches and t = .002 inch

then C = .06286 pf/cm

If $Z_o = 50$ ohms

$$(50)\sqrt{1.6} = \frac{94.15}{\left(\frac{w/2.1}{1-\frac{.002}{2.1}} + \frac{.06286}{(.0885)(1.6)}\right)}$$

$$63.246 = \frac{94.15}{\left(\frac{w}{2.098} + .4439\right)}$$

$$\frac{w}{2.098} + .4439 = \frac{94.15}{63.246}$$

$$w = 2.098\left(\frac{94.15}{63.246} - .4439\right)$$

$$w = 2.192 \text{ inches}$$

The proposed strip dimensions are shown in Figure 7. The required illumination will then determine the spacing between the strips.

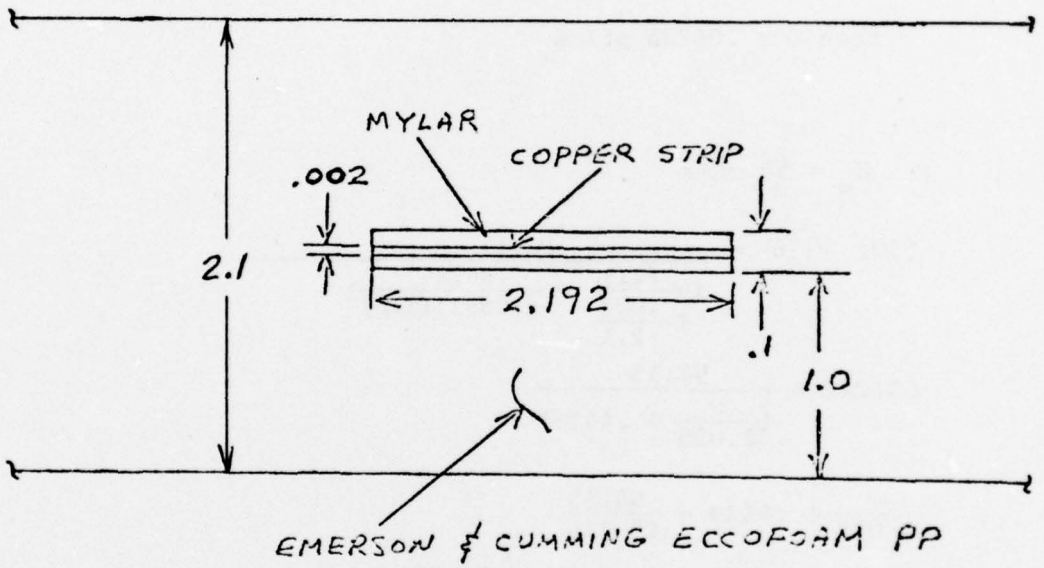

NOTE: DIMENSIONS SHOWN IN INCHES

FIGURE 7

PROPOSED STRIPLINE

Defocused Parabolas

When the insertion loss in stripline becomes large, it is no longer practical to use the stripline method. It is anticipated that 2 GHz is the upper frequency limit. Then, from 2-40 GHz, the field generating system will be defocused parabolas. The test object will be irradiated by antennas which concentrate the radiated energy on the test object a distance 3 meters from the source antenna. To accomplish this requires an antenna system with an effective curved line source. This can be accomplished in a number of ways; a properly phased antenna array, a special shaped reflector or a parabola whose feed is axially defocused. The defocused parabola is the most practical.

The problem with any of the aforementioned approaches, however, is that to illuminate a 3 x 5 foot area at a distance of 3 meters with a 200 V/m field requires signal sources which are expensive because of the output powers required. Since the modeling of the proposed system depends to a great extent upon the available drive power, the following discussion assumes a maximum available power of 100 watts from 2 to 12 GHz and 1 watt from 12 to 40 GHz. In this way, the hardware complexity can be estimated assuming a reasonable design.

Figure 8 is a curve for radiated energy versus resultant field intensity at the beam peak and assumes an antenna of constant electrical aperture, that is, the beamwidth remains constant as a function of frequency. This is an idealized condition, but the resulting curve is useful as an illustration of capability. The problem is set up such that the 6 dB points of the radiated antenna beam intersects the 5 foot dimension of the test object. It can be seen from the curve that 522 watts radiated, produces a field intensity at the peak of the beam of 282.4 V/m (200 V/m + 3 dB) and at the edge of the box, the field intensity will be down 6 dB. This is a field intensity of 141.6 V/m (200 V/m - 3 dB).

Figure 9 is a curve of area illuminated as a function of frequency to generate a 200 V/m field assuming 100 watts radiated from 2-12 GHz and 1 watt radiated from 12-40 GHz. The area represents that area enclosed by a circle whose diameter is equal to the coverage by the H Plane 3 dB beamwidth at 3 meters from the source antenna. The two aforementioned curves are based on far field calculation. A more exact solution of beamwidth and gain in the near field of axially defocused paraboloids has yet to be performed. The 2-40 GHz band will be broken into approximately 11 subbands with reflector sizes varying from 10 to 69 inches in diameter.

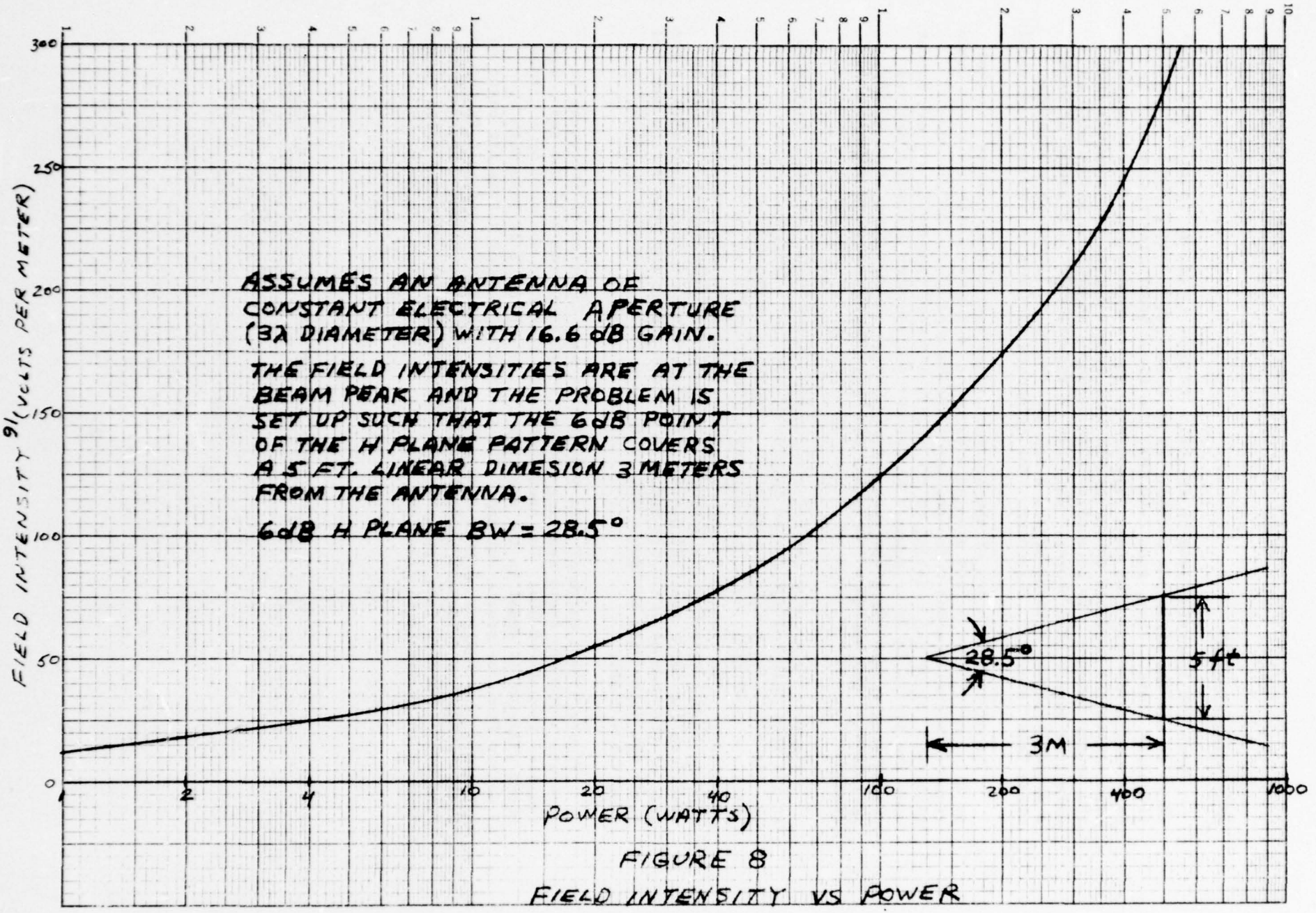

FIGURE 8

FIELD INTENSITY VS POWER

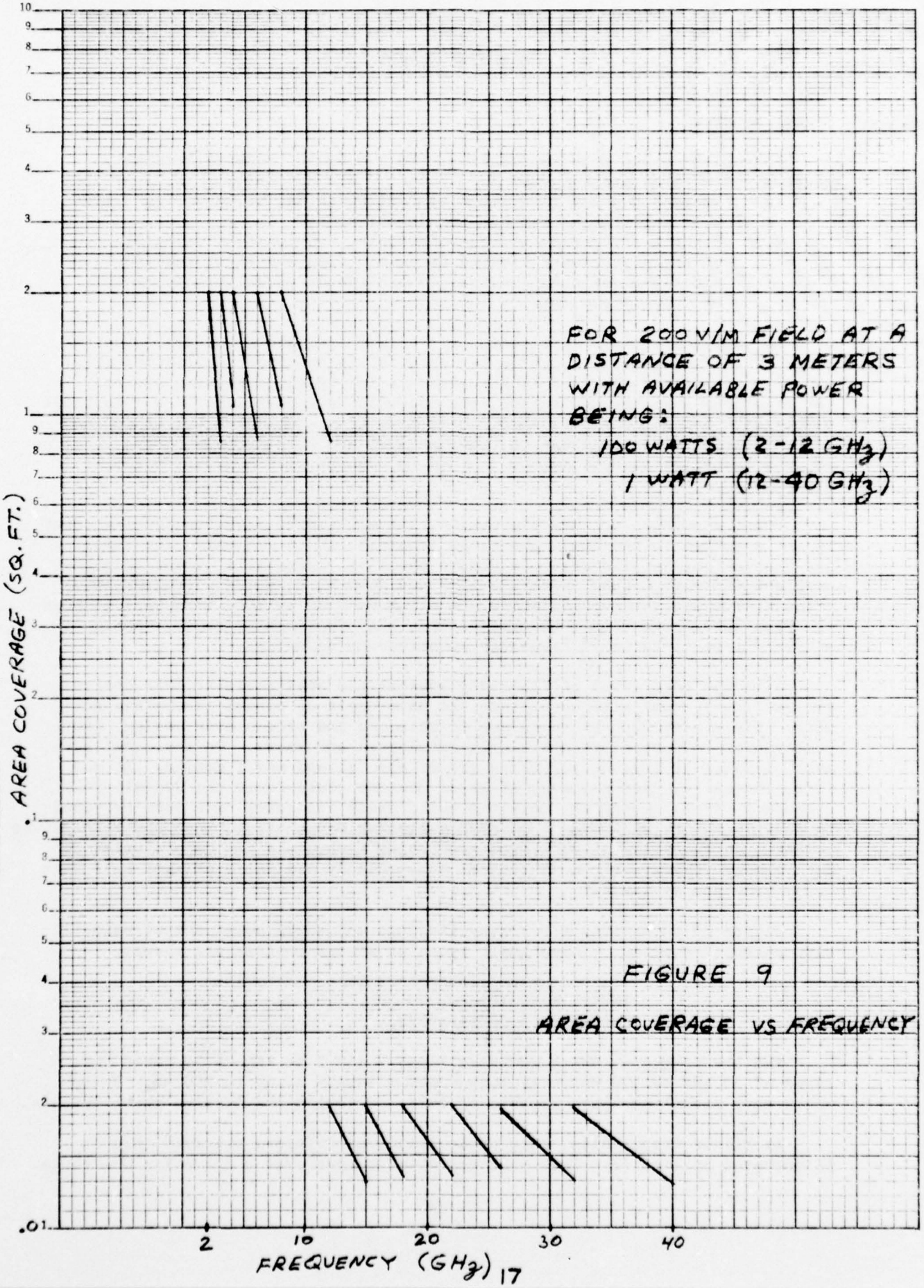

FIGURE 9

AREA COVERAGE VS FREQUENCY

EQUIPMENT SURVEY

Signal Sources

For multi-decade EMRS application, the two basic types of frequency sources under consideration are:

(a) Swept frequency integrated systems which can be tuned over wide frequency ranges without mechanical aids;

(b) Discrete frequency sources of simpler and inexpensive design which operate over limited frequency span and which require additional external devices to provide dc power, tuning control and power leveling.

For millimeter wave application with fixed frequencies or small tuning ranges, klystrons, and more recently, external interaction oscillators (EIO) were almost exclusively used as key elements in signal generating systems. For broadband sweeping and tuning, the backward wave oscillator (BWO) is still widely used and is ideally suited. More recently, stimulated by the development of IMPATT (Impact-Avalanche-Transit-Time) and Gunn or transferred electron devices, solid state oscillators started to compete with conventional millimeter tubes.

For the purpose of this discussion, the millimeter wave frequencies refer to the spectrum in the 30-40 GHz range (that is, 10 to 7.5 mm). The IMPATT and Gunn-effect oscillators have become relatively popular at lower frequencies down through C-Band. Below C-Band and down through audio frequencies, transistor and crystal oscillators are often used as primary frequency sources or, when integrated with tube oscillators, play important circuit function in a hybrid type of variable frequency up-and-down-converters.

Although both types of frequency sources are applicable to EMRS design, the sweeper systems will constitute the main chain of signal generating network. Since many such sweepers are of standard and time-proven design, their performance characteristics are well catalogued and known. On the other hand, most of discrete frequency sources are of special and novel design. It was felt, therefore, that a survey of these devices could cover the overall EMRS frequency range. Moreover, only the solid state discretes have been surveyed to provide a working frame of reference against which all current and near-future advances in the solid state signal generating techniques may be evaluated as EMRS design progresses. Only typical commercially available designs have been considered and evaluated.

Figure 10 summarizes the survey findings and shows power output capabilities versus frequency. Three basic types of signal sources are shown:

Transistorized laboratory-type instruments.
IMPATT oscillators.
Gunn-effect oscillators.

The low frequency units shown as lines 4 and 5 in Figure 10 cover the range of 50 kHz to 520 MHz with output power levels of up to 200 mW. These units have manual sweepers capable of full modulation and leveled power outputs.

At higher frequencies, only phase-locked oscillators are available as illustrated by line 13. This unit has 50 mW output over a 4.3 - 7.7 GHz range.

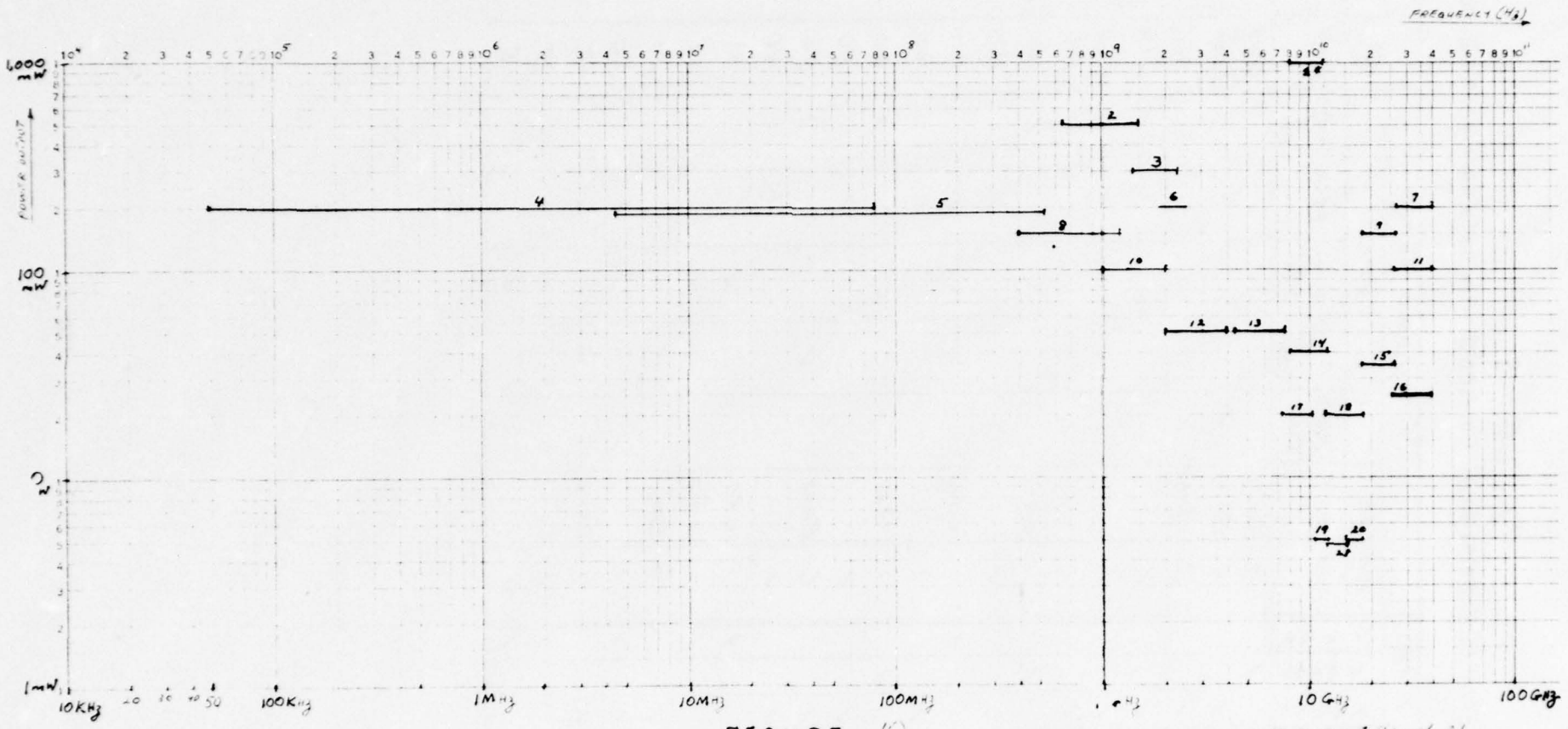

FIGURE 10

SOLID STATE OSCILLATORS & SIG. GENERATORS

*PLOT NOS 1 THROUGH 21 REFER TO DEVICE DESCRIPTION IN TABLE 1

TABLE 1

SURVEY OF SIGNAL SOURCES. EMRS' POWER-FREQ. COVERAGE

PLOT ID #	TYPE			TUNING INFO							P_o MW	FREQ (Hz)	
				RANGE		TYPE							
	TRANSMITTER	IMPATT	GUNN	FULL	PART.	PHASE LOCK	P. LOCK & MULTIP.	E L. VCO	MECH.	MECH & E L.		f_{LOW}	f_{Hi}
1		✓		2-BAND				✓			1,000	8 G	11.5G
2	✓			4-BAND		✓					500	.68G	1.5G
3	✓			2-BAND		✓					300	1.4 G	2.3G
4	✓			✓							200	50K	80M
5	✓			✓							200	4.5M	520M
6	✓			✓		✓					200	1.9G	2.5G
7		✓			0.2G					✓	200	26.5	40G
8	✓			✓					✓		150	0.4	1.2G
9			✓		0.1G				✓		150	18	26 G
10	✓			✓					✓		100	1	2 G
11		✓			3G					✓	100	26.5	40G
12	✓			✓					✓		50	2	4 G
13	✓			6-BAND			✓				50	4.3	7.7G
14	✓			✓					✓		40	8	12.5G
15			✓		0.8G			✓			35	18	26G
16			✓		0.8G			✓			25	26	40G
17	✓			7-BAND			✓				20	7.5	10.5G
18	✓		✓	✓					✓		20	12	18G
19	✓			4-BAND			✓				5	10.47	12.77
20			✓	✓				✓			5	15	18G
21			✓	✓				✓			5	12	15G

Line 18 indicates that only 20 mW output is available over a 12-18 GHz range with units having simpler mechanical tuning design. Line 2 represents a 4-unit phase-locked system capable of 500 mW output over a 0.68 - 1.5 GHz band. Thus, four separate units are required to cover a frequency range of approximately 2.2:1.

The IMPATT diode oscillators are shown by lines 1 and 7. The 1,000 mW unit (line 1) requires two individual assemblies to cover 8-11.5 GHz frequency range. This X-band device is capable of up to 1.5W output power levels. This high power oscillator is voltage-controlled as opposed to line 7 unit which requires both mechanical and electrical tuning to provide a 0.2 GHz frequency change. The latter type is available in the 26.5-40 GHz frequency range with power outputs of 200 mW. The IMPATT devices provide a means of generating several hundred of milliwatts with a minimum number of components. The device needs only a tuned resonant circuit and the proper dc operating voltage. Although the efficiencies of only 10% are attainable at X-band frequencies, these devices represent one of the most efficient means to generate RF power in the 10 GHz frequency region.

Gunn-effect devices, because of their inherent efficiency, reliability, and, particularly portability (as opposed to the tube-type sources), are finding wide application in contactless object detection and observation equipments. The Gunn diode can be made to oscillate in waveguide, coaxial or microstrip circuits by means of a resonator and dc power supply through a low-pass filter.

Figure 10 shows several typical Gunn-effect oscillators in the 15-40 GHz frequency range. The two units in the 12-18 GHz range (lines 20 and 21) are voltage tuned and have bandwidths of 20-25%. Their power output levels are in the order of 5 mW. Higher power levels are obtainable only at considerable sacrifice in bandwidth. A 150 mW unit, shown as line 8 in Figure 10, has a mechanical tuning range of 0.1 GHz. The line 11 IMPATT unit, capable of 100 mW output, could be electro-mechanically tuned over a 3 dB bandwidth of 3 GHz. These broadband devices are available to cover a 26.5-40 GHz range.

Table 1 provides additional description of the most pertinent performance features of the solid state signal sources shown in Figure 10.

Regarding the sweeper systems of (a) above, their main advantage for EMRS application is their broadband integrated system concept that will complement the advanced technology capability of the overall EMRS design. The changes in setups will be minimized and possible alternations of such critical parameters as frequency, sweep width and power level will be reduced. The modern sweepers have the repeatable performance features of accurate laboratory instruments, and, in the advent of a malfunctioning, their replaceability is not a problem.

Regarding the discrete frequency sources (fixed frequency or limited tuning range devices), their main promising application would be in the areas where potential EMRS users would require only a partial narrowband frequency coverage.

Power Output Devices

The log-log plots of Figure 11 show power frequency coverage of several selected devices having potential performance capabilities in meeting EMRS transmitter requirements for the 10 kHz to 40 GHz radiation frequency range. Only three plots (marked N5, N7 and N10) extend below 10 kHz frequency point. These three instruments have capabilities to supply the necessary power levels over the 30 Hz through 10 kHz lower frequencies where only non-radiated outputs are specified. The plots refer to the following four basic types of devices:

EIO	Extended Interaction Oscillators
N	Non-solid state amplifiers.
S	Solid state amplifiers.
T	Traveling-wave tube amplifiers.

The most important performance characteristics considered in this survey were the CW power output level and bandwidth. The trade-offs related to gain, efficiency, dynamic range, size and weight, cost, reliability, etc., will be considered in the near future as a part of the overall transmitter-antenna optimization effort.

The power-frequency data of Figure 11 is also shown in Table 2 with the plot numbers listed in alpha-numerical order. All devices, except EIO, are amplifiers.

The output devices available above 18 GHz are narrowband devices. This is true for the high-powered EIO as discussed in the first quarterly report as well as for the intermediate powered TWT and the low-powered solid state amplifiers. With narrowband devices, many multiplexed sources will be required to cover the 18 GHz to 40 GHz band. Consequently, inquiries were made of various equipment developers as to what devices might be available above 18 GHz in the near future. Although some development effort in this area was expressed, information was very limited and projections as to future equipment capability and availability above 18 GHz are difficult at this time.

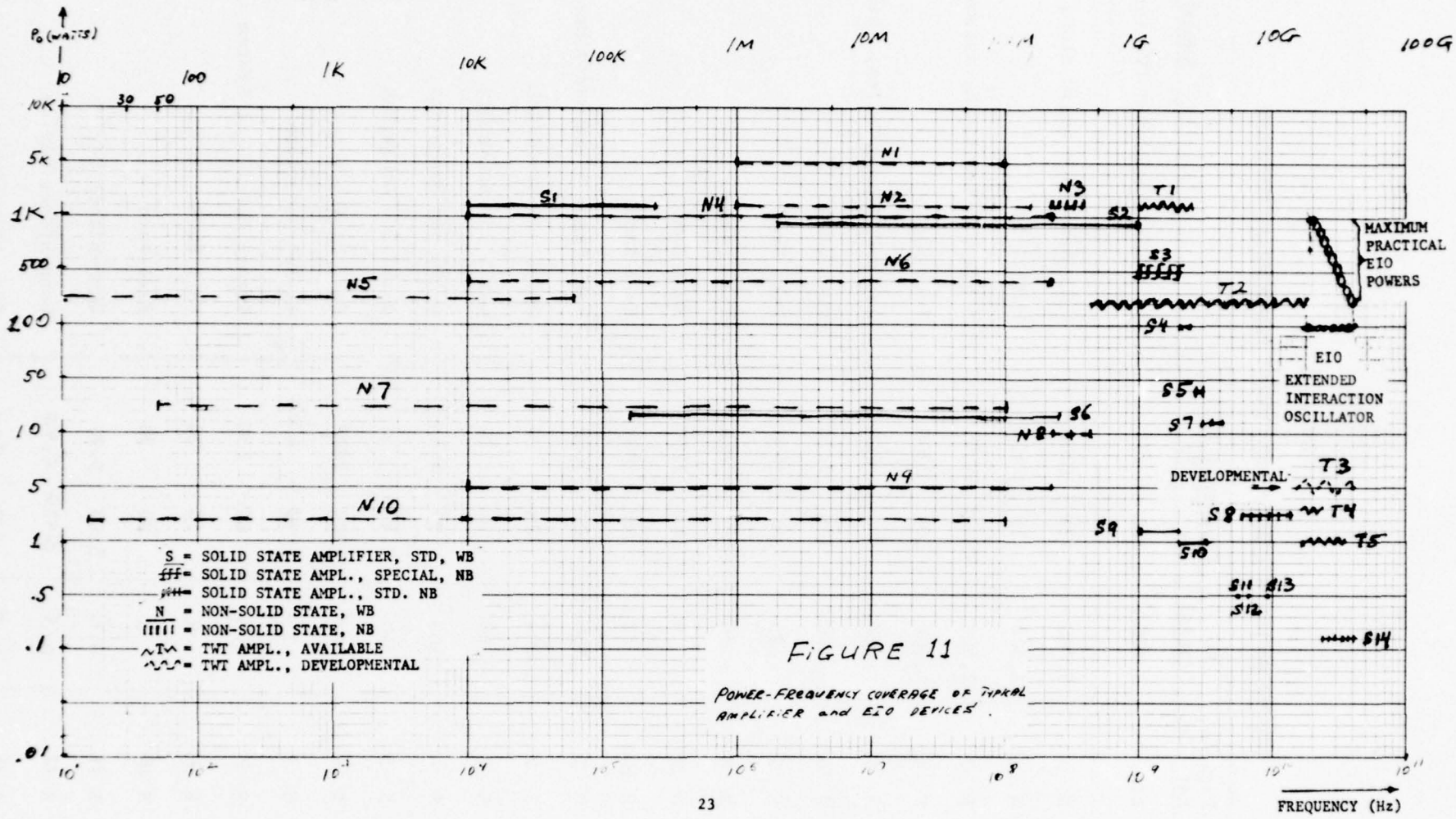

FIGURE 11

POWER-FREQUENCY COVERAGE OF TYPICAL AMPLIFIER and EIO DEVICES.

TABLE 2

SURVEY OF POWER AMPLIFIERS, EMRS' POWER-FREQ. COVERAGE

Fig. 11 Ref No.	Po (Watts)	Frequency (Hz) Fl	Fh	Remarks
EIO	100	18G	40G	4% tunable bandwith (Varian Extended (Interaction OSC.)
N 1	5,000	1M	100M	Full Band. Non-solid state design
N 2	1,500	1M	160M	Full Band
N 3	1,500	225M	400M	4 MHz 3dB-Bandwidth, narrowband
N 4	1,000	10K	220M	Full Band
N 5	250	1	60K	Audio Power Amplifier, full Band
N 6	400	10K	220M	Full Band
N 7	25	50	100M	Full Band
N 8	10	225M	410M	Full Band
N 9	5	10K	220M	Full Band
N 10	2	16	100M	Full Band
S 1	1,100	10K	250K	Full Band. Solid State Design
S 2	1,000	2M	1G	4-10% 3dB-Bandwidth
S 3	500	1G	2G	4-10% 3dB-Bandwidth
S 4	100	2G	2.4G	4-10% 3dB-Bandwidth
S 5	40	2.4G	3G	4-10% 3dB-Bandwidth
S 6	25	150K	250M	Full Band
S 7	15	3G	4.2G	4% 3dB Bandwidth
S 8	2.4	6G	15G	Impatt Multi-Unit System
S 9	2	1G	2G	Full Band
S 10	1	2G	3G	Full Band
S 11	0.5	5.4G	5.9G	Gunn-Effect Device
S 12	0.5	5.92G	6.4G	Gunn-Effect Device
S 13	0.5	8.5G	9.6G	Gunn-Effect Device

Table 2 (continued)

SURVEY OF POWER AMPLIFIERS, EMRS' POWER-FREQ. COVERAGE

Fig. 11 Ref No.	Po (Watts)	Frequency (Hz)		Remarks
		Fℓ	Fh	
S 14	0.15	26G	40G	Gunn-Effect Device, Multi-Unit Assy
T 1	1,500	1G	2.5G	TWT Amplifier, Single Unit Assy
T 2	200	450M	18G	Approx. 2:1 Unit-BW; 5-Unit System
T 3	5	17G	40G	Developmental TWTA's; 1-2 yr D&D cycle
T 4	3	17G	21G	Full Band
T 5	1	18G	26G	Full Band

CONCLUSIONS

The conclusions derived from the second quarter of the design phase are as follows:

- The strip transmission line is proposed as the field generating device at the lower frequencies (up to perhaps 2 GHz); main advantages are minimum drive power requirements and versatility of operation.

- The elliptical reflector cannot produce higher power densities than those existing in the feed-beam of its source and is, therefore, eliminated in favor of the defocused parabola above 2 GHz. With a defocused parabola, beam focusing can be realized as with the elliptical reflector without resorting to specially designed reflectors.

- The EMRS design will be most complex at the upper frequencies because of the lack of wide band devices above 18 GHz.

RECOMMENDATIONS

The updated EMRS block diagram is shown in Figure 12 and shows the recommended equipment configuration to drive the proposed strip transmission line and defocused parabolic reflectors.

The choice in amplifier and/or signal generator selection shown is a practical means of achieving varying user requirements. The choice of signal generators will provide full EMRS capability over discrete frequency ranges, and the choice of amplifiers will provide for different upper level limits for both the radiated and non-radiated outputs.

Further analysis is recommended to completely justify and define the strip transmission line and the defocused parabolic reflector as candidate systems to produce the required field intensities for the EMRS.

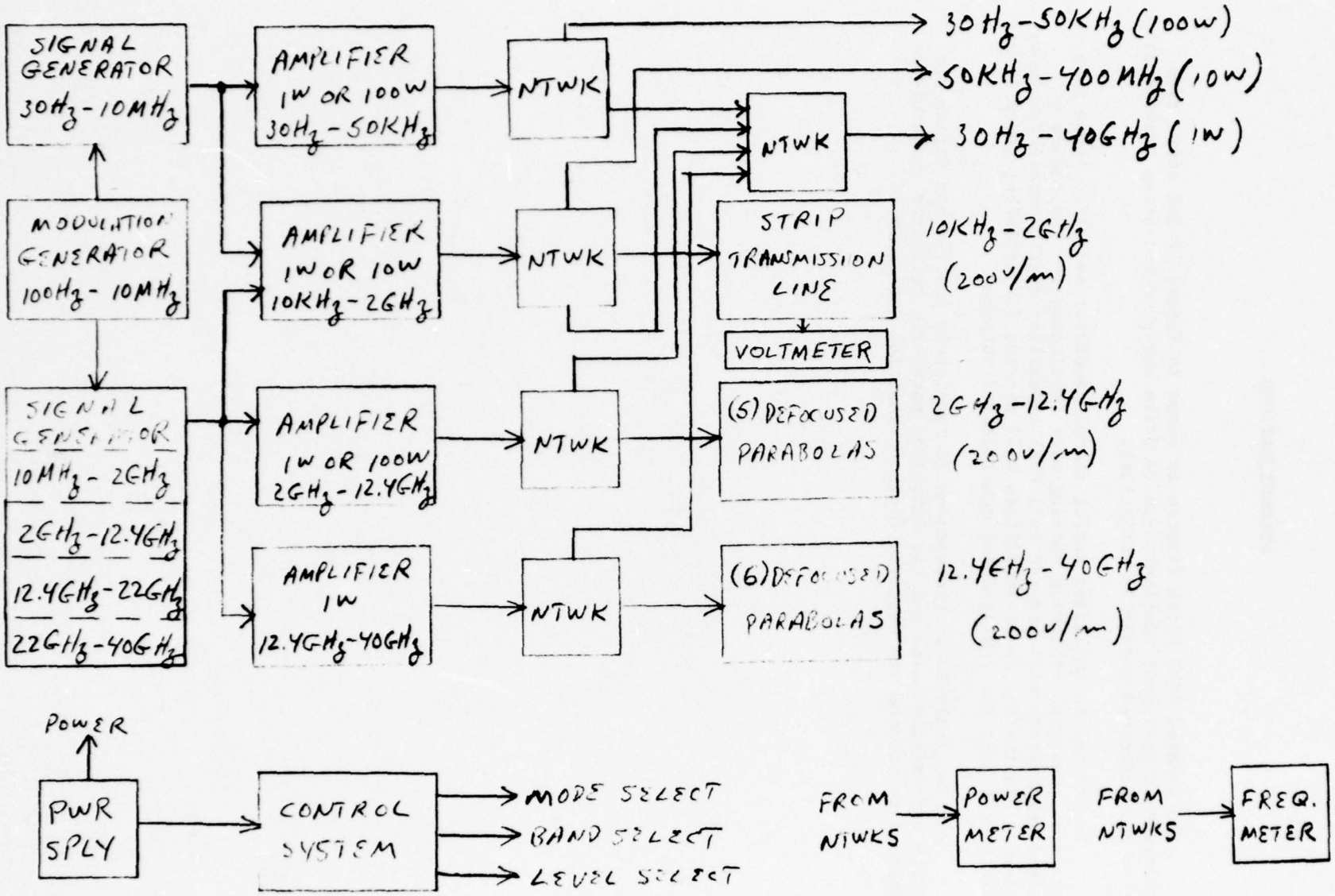

FIGURE 12 EMRS BLOCK DIAGRAM

APPENDIX

ANALYSIS OF PATH-LENGTH DISPERSION IN REFOCUSING BY AN ELLIPSOID-SEGMENT

Prepared by: D.M. Lipkin

ANALYSIS OF PATH-LENGTH DISPERSION IN REFOCUSING BY AN ELLIPSOID-SEGMENT

("For Fixed P, and for P' on the Segment, How Much Does (r'+s) Vary as P' is Moved all Over the Segment?")

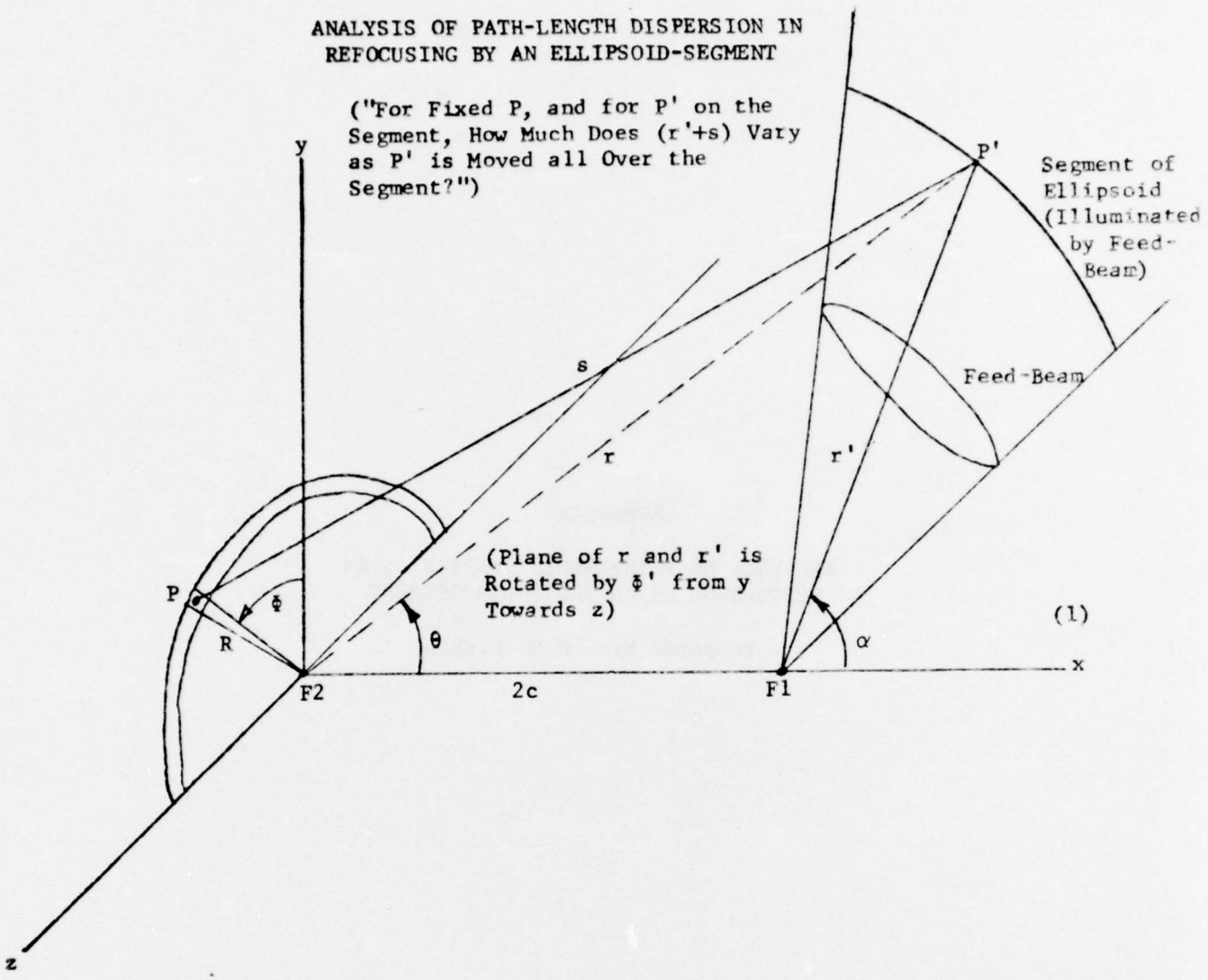

(1)

(Semi-Major Axis of Ellipsoid) ≡ a (2)

(Both Semi-Minor Axes of Ellipsoid) ≡ b < a (3)

$$c = \sqrt{a^2 - b^2} \tag{4}$$

$$\text{Eccentricity "e"} = \left(\frac{c}{a}\right) \tag{5}$$

$$\left(\frac{b}{a}\right) = \sqrt{1 - e^2} \tag{6}$$

A trivially simple - appearing equation which defines the ellipsoid of interest is:

$$(r + r') = 2a \tag{7}$$

and this can be interpreted, in dual polar coordinates, by means of:

$$(r \sin \theta) = (r' \sin \alpha) \tag{8}$$

plus

$$(r \cos \theta) = (2c + r' \cos \alpha). \tag{9}$$

Useful parametric equations for the ellipsoid, derivable from the above, are:

$$\begin{cases} \cos \theta = \left(\dfrac{1 + m \cos \alpha}{m + \cos \alpha}\right) \text{ and} & (10) \\ \sin \theta = \left(\dfrac{n \sin \alpha}{m + \cos \alpha}\right), \text{ with } \alpha \text{ as the independent parameter;} & (11) \end{cases}$$

$$\begin{cases} \cos \alpha = \left(\dfrac{m \cos \theta - 1}{m - \cos \theta}\right) \text{ and} & (12) \\ \sin \alpha = \left(\dfrac{n \sin \theta}{m - \cos \theta}\right), \text{ with } \theta \text{ as the independent parameter;} & (13) \end{cases}$$

$$\begin{cases} r = \left[\dfrac{a (1 - e^2)}{(1 - e \cos \theta)}\right], \text{accompanying (12) and (13),} & (14) \\ r' = \left[\dfrac{a (1 - e^2)}{(1 + e \cos \alpha)}\right], \text{ accompanying (10) and (11);} & (15) \end{cases}$$

and, note that:

$$\left(\frac{d\alpha}{d\theta}\right) = \left(\frac{m + \cos \alpha}{n}\right) = \left(\frac{r}{r'}\right) \equiv K(\alpha), \text{ for later reference.} \tag{16}$$

In all of these, the simplifying notation has been used:

$$\begin{cases} m \equiv \left(\dfrac{\frac{1}{e} + e}{2}\right) \text{ and} & (17) \\ n \equiv \left(\dfrac{\frac{1}{e} - e}{2}\right), \text{where the constant parameter e is the} & (18) \end{cases}$$

eccentricity of the ellipsoid as defined in equation (5). Also note the following algebraic formulas which apply:

NOTE: $m^2 = (1 + n^2)$, $(m + n) = (\frac{1}{e})$, $(m - n) = e$. (19)

The rectangular coordinate locations of P and P' are:

$$P \equiv (0,\ R\cos\Phi,\ R\sin\Phi), \tag{20}$$

$$P' \equiv (r\cos\theta,\ r\sin\theta\cos\Phi',\ r\sin\theta\sin\Phi'). \text{ Therefore,} \tag{21}$$

$$s^2 = [(r\cos\theta)^2 + (r\sin\theta\cos\Phi' - R\cos\Phi)^2 + (r\sin\theta\sin\Phi' - R\sin\Phi)^2] \tag{22}$$

or,

$$s^2 = [r^2 + R^2 - 2rR\sin\theta\cos(\Phi' - \Phi)], \tag{23}$$

or, still further via (7), (8), (15), (17), (18) and (19):

$$s^2 = \left[R^2 - \left|\frac{2a(1-e^2)R\sin\alpha}{(1+e\cos\alpha)}\right|\cos(\Phi' - \Phi) + 4a^2e^2\left(\frac{m+\cos\alpha}{1+e\cos\alpha}\right)^2\right]. \tag{24}$$

From this and (15):

$$(r' + s) = \left[\frac{a(1-e^2)}{(1+e\cos\alpha)} + \sqrt{R^2 - \frac{2a(1-e^2)R\sin\alpha\cos(\Phi'-\Phi)}{(1+e\cos\alpha)} + 4a^2e^2\left|\frac{m+\cos\alpha}{1+e\cos\alpha}\right|^2}\right] \tag{25}$$

Expanded to the second order in $(R/a(1-e^2)) \ll 1$ as a small quantity, Equation (25) gives:

$$(r'+s) = \left\{2a - \left[\frac{2n^2 ae\sin\alpha\cos(\Phi'-\Phi)}{(m+\cos\alpha)}\right]u + \left[\frac{ean^2(1+e\cos\alpha)}{(m+\cos\alpha)}\left(1 - \left|\frac{n^2\sin^2(\alpha)\cos^2(\Phi'-\Phi)}{(m+\cos\alpha)^2}\right|\right)\right]u^2 + (\text{higher order terms in } u)\right\}, \tag{26}$$

where

$$u \equiv \left(\frac{R}{(1-e^2)}\right)\cdot\frac{1}{a} \tag{27}$$

A sufficient condition for the expansion (26) to be valid, and for the term in (μ^2) in (26) to be of negligible importance compared to the term in μ, is simply:

$$\mu \ll 1, \quad \underline{\text{i.e.}}, \quad R \ll (1-e^2)a. \tag{28}$$

Therefore, subject to (28), (26) reduces approximately to: (eliminate μ in favor of R, via (27))

$$(r'+s) \approx \quad (2a) - \left|\frac{R \sin\alpha \cos(\bar{\varphi}'-\bar{\varphi})}{K(\alpha)}\right| \quad , \tag{29}$$

where "$K(\alpha)$" is as defined in (16).

Since the major-axis length (2a) is a constant, independent of α, $\bar{\varphi}$, and $\bar{\varphi}'$, it can be omitted from (29) because it does not contribute to the dispersion of $(r'+s)$ (versus α, $\bar{\varphi}$, and $\bar{\varphi}'$). Thus, we can write, from (29):

$$[\text{dispersion of } (r'+s)] \approx R \cdot [\text{dispersion of} \left|\frac{\sin\alpha \cos(\bar{\varphi}'-\bar{\varphi})}{K(\alpha)}\right|] \tag{30}$$

The general unit direction-vector from F1 to P' (i.e., the vector specified by $(\alpha, \bar{\varphi}')$) is, in retangular coordinates:

$$(\cos\alpha, \sin\alpha \cos\bar{\varphi}', \sin\alpha \sin\bar{\varphi}'); \tag{31}$$

Consider a feed-beam or source-beam, at F1, whose center points along the particular direction $(\alpha_o, \bar{\varphi}'=o)$, i.e., along the unit vector:

$$(\cos\alpha_o, \sin\alpha_o, 0). \tag{32}$$

The cosine of the angle between a general direction (31) at F1, and the beam-center direction (32), is given by the scalar product of the vectors (31) and (32); i.e.:

[cosine of the angle by which (31) is off the center of the feed-beam]

$$= (\cos\alpha \cos\alpha_o + \sin\alpha \sin\alpha_o \cos\bar{\varphi}'). \tag{33}$$

Suppose, now, that the relative-power pattern of the feed-beam is:

$$[\text{cosine (angle off center of beam)}]^N \tag{34}$$

where , e.g.,

$$N = 4.8, \text{ (corresponding to half-power-density angle of } \approx 30^{o}), \tag{35}$$

or other value of interest; then, the relative power pattern, according to (33) and (34), will be:

$$\text{"}P(\alpha, \Phi'; \alpha_o)\text{"} \equiv (\cos\alpha \cos\alpha_o + \sin\alpha \sin\alpha_o \cos\Phi')^N. \tag{36}$$

For small increments $d\alpha$, $d\Phi'$, the solid-angle covered by the increments is:

$$d\Omega \equiv (\sin\alpha \, d\alpha \, d\Phi'). \tag{37}$$

Over a given range ρ of α and Φ', the dispersion (30) can be evaluated as a standard deviation, weighted by $\sqrt{P}$ of (36) and by $d\Omega$ of (37):

$$\Delta \equiv [\text{dispersion of } (r'+s)] =$$

$$= \sqrt{\frac{(\iint_\rho f^2 \sqrt{P}\, d\Omega)}{(\iint_\rho \sqrt{P}\, d\Omega} - \left(\frac{\iint_\rho f \sqrt{P}\, d\Omega}{\iint_\rho \sqrt{P}\, d\Omega}\right)^2} \quad , \tag{38}$$

where f denotes:

$$f \equiv \left[\frac{R \sin\alpha \cos(\Phi'-\Phi)}{K(\alpha)}\right] \quad , \tag{39}$$

the quantity whose dispersion is of interest according to (30).

Therefore,

$$\Delta = \left(\frac{R}{\iint_\rho \sqrt{P}\, d\Omega}\right) \cdot$$

$$\sqrt{(\iint_\rho \sqrt{P}\, d\Omega) \iint_\rho \left(\frac{\sin^2(\alpha) \cos^2(\Phi'-\Phi)}{K^2(\alpha)} \sqrt{P}\, d\Omega\right) - \left(\iint_\rho \frac{\sin\alpha \cos(\Phi'-\Phi)}{K(\alpha)} \sqrt{P}\, d\Omega\right)^2} \tag{40}$$

By using (36), (37) and (16) to expand (40), (40) can be put into the form:

$$\Delta = \left(\frac{nR}{I_o}\right) \sqrt{I_o I_2 - I_1^2} \quad , \tag{41}$$

in which Io, I_1 and I_2 are three integrals defined as follows:

$$\begin{cases} I_o \equiv \iint_\rho [\cos\alpha\cos\alpha_o + \sin\alpha\sin\alpha_o\cos\Phi']^{N/2}\sin\alpha\,d\alpha\,d\Phi', & (42) \\ I_1 \equiv \iint_\rho \left[\dfrac{\cos(\Phi'-\Phi)\,[\cos\alpha\cos\alpha_o+\sin\alpha\sin\alpha_o\cos\Phi']^{N/2}\sin^2(\alpha)}{(m+\cos\alpha)}\right]d\alpha\,d\Phi' & (43) \\ I_2 \equiv \iint_\rho \left[\dfrac{\cos^2(\Phi'-\Phi)\,[\cos\alpha\cos\alpha_o+\sin\alpha\sin\alpha_o\cos\Phi']^{N/2}\sin^3(\alpha)}{(m+\cos\alpha)^2}\right]d\alpha\,d\Phi' & (44) \end{cases}$$

In order to approximate the above integrals conveniently, the weight-function $(\ldots)^{N/2}$ will be set equal to unity (as if N were zero); but, corresponding to (35), the variables α and Φ' will be taken to vary from (α_o-30^o) to (α_o+30^o), and from -30^o to $+30^o$, respectively since this corresponds to the feed beamwidth under consideration. Thus, (42)-(44) are replaced by the rough approximations:

$$I_o^{(ap.)} = \left[\int_{\alpha_o-30^o}^{\alpha_o+30^o} \sin\alpha\,d\alpha \int_{-30^o}^{30^o} d\Phi'\right], \qquad (45)$$

$$I_1^{(ap.)} = \left[\int_{\alpha_o-30^o}^{\alpha_o+30^o} \frac{\sin^2(\alpha)\,d\alpha}{(m+\cos\alpha)} \int_{-30^o}^{30^o} \cos(\Phi'-\Phi)\,d\Phi'\right] \qquad (46)$$

and,

$$I_2^{(ap.)} = \left[\int_{\alpha_o-30^o}^{\alpha_o+30^o} \frac{\sin^3(\alpha)\,d\alpha}{(m+\cos\alpha)^2} \int_{-30^o}^{30^o} \cos^2(\Phi'-\Phi)\,d\Phi'\right]. \qquad (47)$$

Now, (45) is readily evaluated to be: ($30^o = \pi/6$ radians)

$$I_o^{(ap.)} = \left(\frac{\pi}{3}\sin\alpha_o\right). \qquad (48)$$

Similarly, (46) is evaluated to be:

$$I_1^{(ap.)} = \left[\frac{\pi}{3}m - \cos\alpha_o - 2\sqrt{m^2-1}\arctan\left(\frac{\sqrt{m^2-1}}{m\sqrt{3}+2\cos\alpha_o}\right)\right]\cos\Phi \qquad (49)$$

Finally, (47) is evaluated more simply, to be:

$$I_2^{(ap.)} = \left\{ \left[2m \ln \left(1 + \frac{2 \sin \alpha_o}{2m - \sin \alpha_o + \sqrt{3} \cos \alpha_o} \right) - \left(1 + \frac{(m^2-1)}{(m^2-\frac{1}{4}) + m\sqrt{3} \cos \alpha_o + \cos^2 (\alpha_o)} \right) (\sin \alpha_o) \right] \cdot \left[\frac{\pi}{6} + \frac{\sqrt{3}}{4} \cos (2\Phi) \right] \right\} \qquad (50)$$

The standard deviation or dispersion that "Δ" of (38) and (41) represents, can now be evaluated by using the order-of-magnitude approximations (48)-(50).

The type of probability-distribution, of the various lengths (r'+s) whose standard deviation (from-their-own-mean) is Δ, is not immediately known; but, in keeping with the order-of-magnitude approximations being attempted, it seems reasonable to idealize this distribution as Gaussian: With μ representing deviation-from-the-mean, of the (r'+s) values, i.e.,

$$\mu \equiv [(r'+s) - \overline{(r'+s)}], \qquad (51)$$

the probability-distribution of the various μ-values will here be assumed to be representable by the usual normalized Gaussian distribution:

$$\left[\frac{1}{\Delta \sqrt{2\pi}} \exp -\left(\frac{\mu^2}{2\Delta^2} \right) d\mu \right], \qquad (52)$$

in which the same Δ as above plays the role of the standard deviation, and in which the variable μ takes the mathematical range of all real values.

Now, if scalar waves are regarded as being emitted at F1 and following paths (r'+s) to the point P of interest, their combined phasor amplitudes ("voltage") at P will be a superposition of phase-factors corresponding to the various "(r'+s)"-delays, because we can assume that all paths contribute approximately the same magnitude.

Taking the mean path-length (r'+s) to correspond to a reference phase-delay of transmission, the relative phase delay over any particular path (r'+s) will be:

$$\left(\frac{2\pi}{\lambda}\right) \cdot \left[(r'+s) - \overline{(r'+s)}\right], \text{ (radians)}, \tag{53}$$

where λ is the wavelength of the radiation involved. But, by (51), this relative phase-delay is, just:

$$\left(\frac{2\pi\mu}{\lambda}\right), \text{ (radians)}. \tag{54}$$

The complex phase-factor for transmission over any particular path (r'+s) can then be written as:

$$\exp\left(-j\,\frac{2\pi\mu}{\lambda}\right) \cdot \quad (j \equiv \sqrt{-1}). \tag{55}$$

The various phase-factors (55) for different μ can be combined, with probabilities (52), to give the total "voltage" V accumulated at P by superposition of the (scalar) waves:

$$V = \left[\int_{-\infty}^{\infty} \exp\left(-j\,\frac{2\pi\mu}{\lambda}\right) \cdot \left[\frac{1}{\Delta\sqrt{2\pi}} \exp\left(\frac{-\mu^2}{2\Delta^2}\right)\right] d\mu\right] \tag{56}$$

And, the relative power W at P is calculable from:

$$W = |V|^2. \tag{57}$$

The integral (56) can be rearranged to read:

$$V = \left[\frac{1}{\sqrt{\pi}}\, e^{-\left(\frac{2\pi^2\Delta^2}{\lambda^2}\right)} \int_{-\infty+j\left(\frac{\pi\Delta\sqrt{2}}{\lambda}\right)}^{\infty+j\left(\frac{\pi\Delta\sqrt{2}}{\lambda}\right)} e^{-t^2}\, dt\right] \tag{58}$$

But this last integral equals simply

$$\sqrt{\pi} \tag{59}$$*

Therefore, (58) reduces to:

$$V = \exp\left[-\left(\frac{2\pi^2 \Delta^2}{\lambda^2}\right)\right], \tag{60}$$

whence (57) gives:

$$W = \exp\left[-\left(\frac{2\pi}{\lambda}\Delta\right)^2\right]. \tag{61}$$

At the second focus F2 (i.e., if the point P of interest is taken to be F2), we know that Δ vanishes, because all the paths "(r'+s)" are of equal length and therefore have zero dispersion; and then, (61) gives W=1. Therefore, the formula (61), in general, gives the relative power at an arbitrary point P, normalized to unity at P=F2.

Interest now attaches, not so much to the relative-power pattern (61) [in the y-z plane -- see the Figure (1)], as to the location of its half-power points, i.e., the points where

$$W = 1/2. \tag{62}$$

From (61), these points are described by:

$$\Delta = \left[\frac{\lambda}{2\pi}\sqrt{\ln 2}\right] \tag{63}$$

But, then, by eliminating Δ between (63) and (41), we find:

$$\left(\frac{R}{\lambda}\right) = \left(\frac{\sqrt{\ln 2}}{2\pi n\sqrt{\frac{I_2}{I_o}}\sqrt{1 - \frac{I_1^2}{I_o I_2}}}\right) \tag{64}$$

as the desired expression for the half-power locus.

The convenient approximations (48)-(50) for the three intergals I_o, I_1, I_2 may be used in the numberical evaluation of this formula.

* National Bureau of Standards: Handbook of Mathematical Functions No. 55; Equations 7.1.1 and 7.1.16.

Values of R/λ have been calculated from (64), using (48), (49), (50), (18), (17), for a few different values of α_o and e, and in each case for Φ going from 0^o to 90^o in 15^o-steps. (According to (48)-(50), the pattern of R/λ versus Φ should repeat by symmetry in each quadrant, hence its shape for $0 < \Phi \leq 90^o$ is sufficient to specify its shape for all Φ.)

The results of the numerical calculations are: (Main entries denote R/λ values; see Figure 1 for meaning of R).

Angular Location About 2nd Focus "Φ"	Up-Tilt Angle "α_0" of Center of Feed-Beam					
	45^o	45^o	60^o	60^o	90^o	90^o
	Ellipsoid Eccentricity "e"					
	0.3	0.4	0.3	0.4	0.3	0.4
0^o	.9025	1.0587	.8836	.9847	1.0393	.9483
15^o	.9025	1.0611	.8707	.9761	.9575	.9069
30^o	.9026	1.0678	.8381	.9538	.8056	.8165
45^o	.9028	1.0771	.7990	.9257	.6810	.7278
60^o	.9029	1.0867	.7648	.8999	.6007	.6629
75^o	.9031	1.0939	.7424	.8823	.5571	.6251
90^o	.9031	1.0965	.7347	.8761	.5434	.6128

(65)

(The computations were run automatically on an HP-9820A programmable desk calculator.)

The results in the table (65) indicate, qualitatively, that the region of imperfect focusing around the illipsoid's second ideal focus is always of the order of 1/2 to 1 wavelength in radius (and is not circular, in general).

Since the actual source of the feed-beam is not a geometrical point, the above "circle-of-confusion" figures are most likely smaller-than-actual.

Also, since the source itself need not generally (for the 30^{o} half-beam angle assumed) have a radius as large as $\lambda/2$, the power-density at the second focus will not be as large as that in the aperture of the source. Thus, although "focusing" occurs, it cannot produce higher power densities than those existing in the feed-beam at its source-aperture (this conclusion holds for all λ). The basic physical reason for this is, that although the conditions for focusing of radiation are not met with mathematical exactitude at points that deviate from the second focus, the lack of perfect focusing at such points does not become serious until the points are more than about $\lambda/2$, or λ, removed from the ideal focus; this is a general feature of wave-interference which must be considered in practical situations.

DISTRIBUTION LIST

101 Defense Documentation Center
ATTN: DDC-TCA
Cameron Station (Bldg 5)
*012 Alexandria, VA 22314

104 Defense Communications Agency
Technical Library Center
Code 205
001 Washington, DC 20305

107 Director
National Security Agency
ATTN: TDL
001 Fort George G. Meade, MD 20755

108 Director, Defense Nuclear Agency
ATTN: Technical Library
001 Washington, DC 20305

110 Code R121A, Tech Library
DCA/Defense Comm Engring Ctr
1860 Wiehle Ave
001 Reston, VA 22090

200 Office of Naval Research
Code 427
001 Arlington, VA 22217

201 Commander, Naval Ship Sys Cmd
Technical Library, RM 3 S-08
National Center No. 3
001 Washington, DC 20360

202 Naval Ships Engineering Center
Code 6157D
Prince Georges Center
001 Hyattsville, MD 20782

205 Director
Naval Research Laboratory
ATTN: Code 2627
001 Washington, DC 20375

206 Commander
Naval Electronics Lab Center
ATTN: Library
001 San Diego, CA 92152

207 Commander
US Naval Ordnance Laboratory
ATTN: Technical Library
001 White Oak, Silver Spring, MD 20910

210 Commandant, Marine Corps
HQ, US Marine Corps
ATTN: Code LMC
001 Washington, DC 20380

211 HQ, US Marine Corps
ATTN: Code INTS
001 Washington, DC 20380

212 Command, Control & Comm Div
Development Center
Marine Corps Dev & Educ Cmd
001 Quantico, VA 22134

214 Commander, Naval Air Sys Cmd
Meteorological Div (AIR-540)
001 Washington, DC 20361

215 Naval Telecommunications Cmd
Tech Library, Code 422
4401 Massachusetts Ave, NW
001 Washington, DC 20390

301 Rome Air Development Center
ATTN: Documents Library (TILD)
001 Griffiss AFB, NY 13441

304 Air Force Cambridge Research Lab
L.G. Hanscom Field
ATTN: LIR
001 Bedford, MA 01730

307 HQ ESD (ZRRI)
L.G. Hanscom Field
001 Bedford, MA 01730

312 AFSPCOMMCEN/SUR
001 San Antonio, TX 78243

313 Armament Dev & Test Center
ATTN: DLOSL, Tech Library
001 Eglin Air Force Base, FL 32542

314 HQ, Air Force Systems Cmd
ATTN: DLCA
Andrews AFB
001 Washington, DC 20331

315 Director
Air University Library
ATTN: AUL/LSE-64-285
001 Maxwell AFB, AL 36112

318 HQ, AFCS
ATTN: EPECRW Mail Stop 105B
001 Richards-Gebaur AFB, MO 64030

403 HQDA(DACE-CMS)
001 WASH, DC 20310

405 OSASS-RD
001 WASH, DC 20310

406 Commander
US Army Training & Doctrine Cmd
ATTN: ATCD-SI
001 Fort Monroe, VA 23651

407 Commander
US Army Training & Doctrine CMD
ATTN: ATCD-CI
001 Fort Monroe, VA 23651

408 HQDA(DARD-ARS-P/Dr. R.B. Watson
001 WASH, DC 20310

409 CDR, DARCOM
ATTN: DRCMA-EE
5001 Eisenhower Ave
001 Alexandria, VA 22333

414 Commander
US Army Training & Doctrine Cmd
ATTN: ATCD-F
001 Fort Monroe, VA 23651

417 CDR, DARCOM
ATTN: DRCRD-01 (Mr. Speight)
5001 Eisenhower Ave
001 Alexandria, VA 22333

419 Commander
US Army Missile Command
ATTN: DRSMI-RR, Bldg 7770
001 Redstone Arsenal, AL 35809

421 CDR, US Army Missile Command
Redstone Scientific Info Ctr
ATTN: Chief, Document Section
002 Redstone Arsenal, AL 35809

422 Commander
NS Army Aeromedical Research Lab
ATTN: Library
001 Fort Rucker, AL 36362

423 Commander
US Army Armament Command
ATTN: DRSAR-RDP (Library)
001 Rock Island, IL 61201

427 CDR, US Army Combined Arms
Combat Developments Activity
ATTN: ATCAIC-IE
002 Fort Leavenworth, KS 66027

429 Commander
US Army Logistics Center
ATTN: ATCL-MA
001 Fort Lee, VA 23801

430 Commandant
US Army Ordnance School
ATTN: ATSOR-CTD
001 Aberdeen Proving Ground, MD 21005

431 Commander
US Army Intelligence School
ATTN: ATSIT-CTD
001 Fort Huachuca, AZ 85613

432 Commandant
US Army Field Artillery School
ATTN: ATSFA-CTD
001 Fort Sill, OK 73503

433 CDR, US Army Aviation Sys Cmd
ATTN: DRSAV-G
PO Box 209
001 St. Louis, MO 63166

442 Commander
Harry Diamond Laboratories
ATTN: Library
2800 Powder Mill Rd.
001 Adelphia, MD 20783

448 Commander
Picatinny Arsenal
ATTN: SARPA-ND-A-4 (Bldg 95)
001 Dover, NJ 07801

449 Commander
Picatinny Arsenal
ATTN: SARPA-TS-S #59
002 Dover, NJ 07801

450 Commander
Frankford Arsenal
ATTN: Library, K2400, BL.51-2
001 Philadelphia, PA 19137

452 Commander
Frankford Arsenal
ATTN: SARFA Z1000 (Mr. Kerensky)
001 Philadelphia, PA 19137

455 Commander
White Sands Missile Range
ATTN: STEWS-ID-S HQ
001 White Sands Missile Range, NM 88002

458 Dir/Dev & Engr
Defense Systems Div
ATTN: SAREA-DE-DDR, H. Tannenbaum
002 Edgewood Arsenal, APG, MD 21010

465 Commander
Aberdeen Proving Ground
ATTN: STEAP-TL (Bldg 305)
002 Aberdeen Proving Ground, MD 21005

474 Director
US Army Human Eng Labs
001 Aberdeen Proving Gd, MD 21005

475 Commander
HQ, Fort Huachuca
ATTN: Technical Ref Div
002 Fort Huachuca, AZ 85613

476 Commander
US Army Electronic Proving Gd
ATTN: STEEP-MT
002 Fort Huachuca, AZ 85613

480 Commander
USASA Test & Evaluation Ctr
001 Fort Huachuca, AZ 85613

482 Commander
US Army Communications Command
ATTN: ACC-FD-M
001 Fort Huachuca, AZ 85613

483 Commander
US Army Research Office
ATTN: DRXRO-IP
P.O. Box 12211
001 Research Triangle Park, NC 27709

484 Commander
US Army Research Office
ATTN: Dr. Robert J. Lontz, DRXRO-PH
P.O.Box 12211
001 Research Triangle Park, NC 27709

488 US Army Security Agency
ATTN: IARD
Arlington Hall Station
001 Arlington, VA 22212

489 Commander
US Army Tank-Automotive Command
ATTN: DRSTA-RW-L
001 Warren, MI 48090

490 Commander
Edgewood Arsenal
ATTN: SAREA-TS-L
001 Aberdeen Proving Ground, MD 21010

500 Commander
US Army Yuma Proving Ground
ATTN: STEYP-MTD (Tech Library)
002 Yuma, AZ 85364

505 CDR, US Army Security Agency
ATTN: IARD-T
Arlington Hall Station
001 Arlington, VA 22212

511 Commander
US Army Nuclear Agency
001 Fort Bliss, TX 79916

515 Director
Joint Comm Office (TRI-TAC)
ATTN: TT-AD(Tech Docu Ctr)
001 Fort Monmouth, NJ 07703

517 Commander
US Army Missile Command
ATTN: DRSMI-RE (Mr. Pittman)
001 Redstone Arsenal, AL 35809

519 Commander
US Army Systems Analysis Agency
ATTN: DRXSY-T (Mr. A. Reid)
001 Aberdeen Proving Ground, MD 21005

525 Project Manager, REMBASS
ATTN: DRCPM-RBS
001 Fort Monmouth, NJ 07703

526 Project Manager, NAVCON
ATTN: DRCPM-NC-TM (T. Daniels)
Bldg 2539
001 Fort Monmouth, NJ 07703

596 Commandant
US Army Signal School
ATTN: ATSN-CTD-MS
002 Fort Gordon, GA 30905

598 Commander
US Army Satellite Comm Agency
ATTN: DRCPM-SC-3
001 Fort Monmouth, NJ 07703

599 TRI-TAC Office
ATTN: CSS (Dr. Pritchard)
001 Fort Monmouth, NJ 07703

607 Commander
US Army Tank-Automotive Cmd
ATTN: DRSTA-RHP, Dr. J. Parks
001 Warren, MI 48090

613 Atmospheric Sciences Lab, ECOM
ATTN: DRSEL-BL-SY-L
001 White Sands Missile Range, NM 88002

617 Chief
Intel Material Dev & Support Ofc
Electronic Warfare Lab, ECOM
001 Fort Meade, MD 20755

680 Commander
US Army Electronics Command
000 Fort Monmouth, NJ 07703

1 DRSEL-PL-ST
1 DRSEL-VL-D
1 DRSEL-PP-I-PI
1 DRSEL-WL-D
1 DRSEL-TL-D
3 DRSEL-CT-D
1 DRSEL-BL-D
3 DRSEL-NL-RY-5
1 DRSEL-NL-D-5 (Ofc of Record)
1 DRSEL-SI-CM
1 DRSEL-MA-MP
2 DRSEL-MS-TI
1 DRSEL-GG-TD
1 DRCPM-AA
1 DRSEL-CG (Mr. Doxey)
2 DRSEL-PA
1 DRCPM-TDS-SE
1 USMC-LNO
1 DRSEL-GS-H
1 DRSEL-RD
1 TRADOC-LNO

610 Director, Night Vision Laboratory
US Army Electronics Command
ATTN: DRSEL-NV-D
001 Fort Belvoir, VA 22060

701 MIT-Lincoln Laboratory
ATTN: Library, Rm A-082
P.O. Box 73
001 Lexington, MA 02173

703 NASA Scientific & Tech Info
Facility
ATTN: Acquisitions BR (S-AK/DL)
002 College Park, MD 20740